

CHARACTERISATION AND AUTOMATIC DETECTION OF LYMPH NODES ON MR COLORECTAL IMAGES

Jeong-Gyoo Kim and J. Michael Brady

Dept. Engineering Science, Oxford University, Parks Road, Oxford, UK

Keywords: Medical image analysis, lymph node characterisation, PDF modelling, and segmentation.

Abstract: Colorectal cancer is the second most common cause of death in Western countries. It is often curable by chemoradiotherapy and/or surgery; however, accurate staging has a significant impact on patient management and outcome. Numerous clinical reports attest to the fact that staging is not currently satisfactory, and so more precise methods are required for effective treatment. The three major components of disease staging are tumour size; whether or not there is distal metastatic spread; and the extent of lymph node involvement. Of these, the latter is currently by far the hardest to quantify, and it is the subject of this paper. Lymph nodes are distributed throughout the mesorectal fascia that envelops the colorectum. In practice, they are detected and assessed by clinicians using properties such as their size and shape. We are not aware of any previous image analysis approach for colorectal images that makes this subjective approach more scientific.

To aid precise staging and surgery, we have developed methods that characterises lymph nodes by extracting implicit properties as computed from magnetic resonance colorectal images. We first learn the probability density function (PDF) of the intensities of the mesorectal fascia and find that it closely approximates a Gaussian distribution. The parameters of a Gaussian, fitted to the PDF, were estimated and the mean intensity of a lymph node candidate was compared with it. The fitting provides an explicit criterion for a region to be classed as a lymph node: namely, it is an outlier of the Gaussian distribution.

As a key part of this process, we need to segment the boundaries of the mesorectal fascia, which is enclosed by two closed contours. Clinicians recognise the outer contour as thin edges. Since the thin edges are often ambiguous and disconnected, differentiating them from neighbouring tissues is a non-trivial problem; the surrounding tissues have no significant difference from the mesorectal fascia in both intensity and texture. We employed a level set method to segment three sets of objects: the mesorectal fascia, the colorectum, and lymph node candidates. Our segmentation results led us to build a PDF and to use it for the criterion that we propose. The whole process of implementation of our methods is automatic including the lookup of lymph candidates. The results of clinical cases are summarised in the paper.

1 INTRODUCTION

Colorectal cancer is the second most common cause of death in Western countries (McArdle et al., 2000) and its incidence has increased in many Asian countries over the past few decades (Sung et al., 2005). It is known that the disease is curable by chemoradiotherapy and/or surgery if it is detected at an early stage and treated appropriately; surgery is currently the best curative therapy. Therefore, cancer staging¹ has a significant impact on patient management, not least the decision whether to proceed to surgery.

¹The extent to which a (colorectal) cancer has spread is described as its stage.

Though accurate preoperative staging is essential for planning of optimal therapy, there have been numerous clinical reports which attest to the fact that preoperative staging accuracy based on clinician judgement of images is not satisfactory (Filippone et al., 2004), and so a method for more precise staging is required for patient management and effective treatment. Staging of the disease is based on the TNM classification: tumour size (T); whether or not there is distal metastatic spread (M); and the extent of lymph node involvement (N). Of these, the latter is currently by far the hardest to quantify, and it is the subject of this paper.

Lymph is a clear fluid that travels through the body's arteries, circulates through the tissues to

cleanse them and keep them firm, and then drains away through the lymphatic system. Cancer cells may drain into nearby lymph nodes, which are bean-shaped structures that help fight against infection. Lymph nodes are the filters along the lymphatic system. Since the lymph nodes function to filter out harmful cells, in particular cancer cells, this is a logical place to look for cancer cells that have escaped the original tumor and are seeking to metastasise to a distal location. Lymph node dissection prevents cancer cells from further growth. The number of involved lymph nodes strongly predicts the nature of the cancer and the type of treatment needed to fight it. For these reasons, it is considered by clinicians to be of great importance to assess lymph nodes in the management of cancer.

In the case of colorectal cancer, the lymph nodes appear as dark small blobs on magnetic resonance (MR) images and are distributed mostly in the mesorectum, a fatty tissue that envelops the colorectum. In practice, lymph nodes are characterised by human vision using explicit properties, such as size and shape of lymph nodes. We are not aware of any method of image analysis approach of colorectal images that makes this subjective approach more scientific.

In this paper we develop methods to aid precise staging and estimation of the circumferential resection margin of colorectal cancers, namely detection and characterisation of a lymph node. The contribution of the proposed methods can be divided into two categories: modeling an intensity probability density function (PDF) and segmentation of non-trivial MR images.

Section 2 describes the methods we propose; characterising a lymph node by building a PDF of intensity of the mesorectal fascia. For this purpose, we need to segment the mesorectal fascia on non-trivial images as well as lymph node candidates. Our experiments are presented in section 3, and section 4 concludes and discusses our work.

2 METHODS

Our methods include lymph node detection and characterisation; the two unrelated categories are combined here.

We attempt to detect and analyse lymph nodes from 3D MR colorectal images, taken at our local hospitals by GE 1.5T magnetic resonance imaging scanners with parameters of $TE = 120ms$, $TR = 6500ms$. Each 3D dataset comprises a set of 23 to 30 slices each corresponding to a $3mm$ to $5mm$ slab of

tissue.

Lymph nodes generally appear as small dark blobs, of a distinctively low intensity compared to the surrounding fat which has high intensity. However, lymph nodes may be heterogeneous in intensity: such heterogeneity is generally considered evidence for a lymph node being affected by cancer. Furthermore, since lymph nodes are small and the sampling in MRI is large compared to their size, the partial volume effect (PVE, in which multiple tissue structures are present in a single voxel) has a substantial impact on the intensities at locations that correspond to lymph nodes. Also, the generally bright background is punctuated with folds in the fat, which complicate its appearance. The dark blobs corresponding to lymph appear locally similar to blood vessels, especially when viewed in a single two dimensional slice image. We can eliminate blood vessels on the basis of their three dimensional shapes (extended over several slices). The consecutive slices are registered and examined if they extend over several slices; if so, they are more likely to be blood vessels. As a result, we may estimate locations of some possible lymph node candidates. For each candidate we test our methods described in this section.

Current characterisations of lymph nodes stress either their size and/or shape (Lee et al., 1984; Brown et al., 2003; Bond, 2006). Such criteria are observations of explicit properties, as seen on images. We aim to extract implicit properties of lymph nodes using image analysis techniques, and which can lead to a higher precision of lymph node criteria.

Lymph nodes are distributed in a priori unpredictable locations within the mesorectum. Because they are small, subject to the PVE, and are in unpredictable locations, we first determine information about the surrounding mesorectum and use it to locate the lymph nodes. More precisely, we first model the PDF of the mesorectum. However, to estimate the mesorectum PDF we first need to isolate it from its surrounding tissues.

The dark round object at the lower center in Figure 1 is the colorectum. The object of higher intensity that envelops the colorectum is the mesorectum, bound by the mesorectal fascia. The mesorectal fascia can be recognised by human vision as a very thin low signal intensity, however, because of the low signal to noise and the poor sampling density, edge detectors tend to produce disconnected edges.

To isolate the mesorectum, we need to delineate the boundary of the mesorectal fascia and the boundary of the colorectum. The difficulty of this segmentation task derives from the fact that there is, in several places, no intensity or texture difference between the

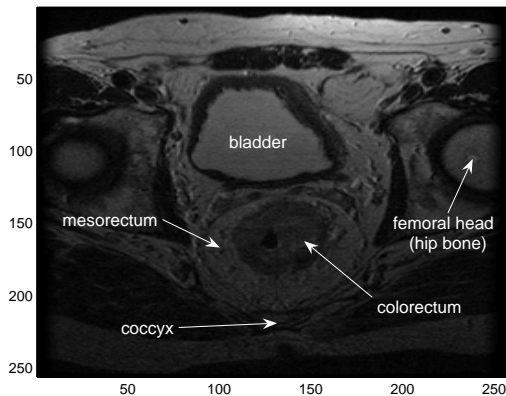


Figure 1: A slice of an MR colorectal image: off-plane axial view.

mesorectal fascia and surrounding tissues along the thin edges. The shape of the mesorectal fascia varies from patient to patient, as do the slice locations of the patient.

Subsection 2.1 presents how we characterise lymph nodes, while subsection 2.2 presents delineation of the mesorectum and lymph nodes using level set methods. The criteria on an automatic lookup of lymph candidates are discussed in 2.3.

2.1 Characterisation of Lymph Nodes

As explained earlier, we try to extract implicit properties of lymph nodes that can be read from images. The most common way of extracting a property of image could be its intensity. We have examined simple statistics of the intensity of the mesorectum such as moments: mean, variance, skewness and Kurtosis. We found that such statistics are inadequate to differentiate lymph nodes from the mesorectum.

For this reason, we first learn the intensity probability distribution function (PDF) of the mesorectal fascia. This PDF is likely to be Gaussian as has been frequently noted, for example (Cremers, 2006). We have found that the PDF closely approximates a Gaussian distribution $N(\mu, \sigma^2)$. We also tested the Rayleigh distribution (since this is ideally the noise model for MRI), but we found that it was not as good a fit to the intensity histogram as a Gaussian. The parameters μ and σ^2 of the Gaussian distribution vary from patient to patient, so they should be estimated for each individual.

We model the PDF with

$$\mathcal{P}(x) \approx \alpha \exp\left\{-\frac{(x-\mu)^2}{2\sigma}\right\} \quad (1)$$

where $\exp\{\cdot\}$ is an exponential function. This re-

quires the fitting of the three parameters ² α , μ and σ to the intensity histogram. The candidate lymph nodes can be differentiated from the mesorectal fascia using the PDF. We know a priori that the lymph nodes are darker than fat voxels in the mesorectal fascia and so their intensity will fall into a range on the left tail of the Gaussian curve. We have found in our experiments that the lymph nodes are clustered around, or below, $\mu - 2\sigma$ of the estimated Gaussian curve in equation (1). That is, our criterion for finding a candidate lymph node is that it should be an outlier of the Gaussian estimated with equation (1).

To utilise this characterisation method, we need to segment the boundaries of the mesorectum, as discussed in the next subsection.

2.2 Detection of Lymph Nodes

As shown in Figure 1, the edges of the inner contour of the mesorectum, i.e., the boundary of the colorectum, is rather clear. However, the outer boundary of the mesorectum, the mesorectal fascia is very ambiguous. We have tested various methods to segment the the mesorectal fascia, such as the EM algorithm, hidden Markov random measure fields (Marroquin et al., 2003), phase congruency (Felsberg and Sommer, 2001), and anisotropic diffusion (Perona and Malik, 1990). All these methods have performed well on other images such as brain images. However, they performed considerably less well on our colorectal images, partly because of the poor signal to noise and partly because of ambiguous boundaries. We needed a method to segment extremely thin edges and have found that level set methods had superior performance to all the other methods of segmentation. Level set methods are briefly introduced next.

2.2.1 Level Set Methods for Segmentation

There have been numerous papers on segmentation using the level set methods in image analysis areas

²The scale factor α is remained in our expression to approximate the PDF \mathcal{P} since we do not normalise the Gaussian, say $G(\alpha, \mu, \sigma)$. When normalised (i.e. the area below the Gaussian curve in the upper half plane is 1), it can be expressed by two parameters $G(\mu, \sigma)$ with the scale factor $\frac{1}{\sqrt{2\pi\sigma}}$. One can use any of the both expressions for optimisation. In order to find optimal parameters, we used line search, which is based on the gradient of $G(\alpha, \mu, \sigma)$, and the partial derivatives $\frac{\partial G}{\partial \alpha}$, $\frac{\partial G}{\partial \mu}$ and $\frac{\partial G}{\partial \sigma}$ are computed. Since the function $G(\alpha, \mu, \sigma)$ is linear with respect to α and σ appears only in $\exp(\cdot)$, this separation of the scale factor makes $\frac{\partial G(\alpha, \mu, \sigma)}{\partial \sigma}$ simpler than $\frac{\partial G(\mu, \sigma)}{\partial \sigma}$ which tends to be easily perturbed by a small change of σ and optimisation is prone to fail with.

since the early work in the 90's such as Malladi *et al.* (Malladi et al., 1995) and Caselles *et al.* (Caselles et al., 1997). One of the well known advantages of such methods is that they are able to model topological changes of boundaries of objects, merging and splitting, during the evolution of an embedded function (Sethian, 1999).

Within the level set framework of Osher and Sethian (Osher and Sethian, 1988), various types of energy functionals are employed (Chan and Vese, 2001; Paragios and Deriche, 2000; Yezzi and Soatto, 2003; Li et al., 2005). Most researchers use a signed distance function for an initial ϕ ; but recently some have suggested that the initial function does not have to be a distance function. With alternative types of initial functions such as piecewise constant functions, Lee and Seo (Lee and Seo, 2006) and the work of D. Cremers's group have demonstrated successful implementations of level set methods.

We adopted the model proposed by Chan and Vese (Chan and Vese, 2001), since it has shown superior performance on our colorectal images to other level set models. The model is not based on the image gradient of the image to stop the process, but is based on the segmentation techniques of Mumford-Shah functional (Mumford and Shah, 1989). The fitting term of their energy functional is designed to be minimised when the segmented contour is on the boundary of the object; the regularisation term is defined by the area of the region inside the segmented contour and its length. The model does not need to smooth the raw image for segmentation, which is required in many other segmentation methods. When smoothed, the very thin edges on our data sets were buried into the surrounding tissues and this resulted in poor performance of segmentation. The model generally copes well with the objects of ambiguous boundaries or reasonably noisy boundaries on images.

2.2.2 Segmentation of the Mesorectal Fascia

Chan and Vese (Chan and Vese, 2001) assume that the intensity of an image can be approximated by a piecewise constant function $u : \bar{\Omega} \rightarrow \mathbb{R}$ as do many other segmentation techniques. In a simple case, a grey image can be represented by a binary image, having two values of intensity, and the locations $(x, y) \in \Omega$ where there is a jump in the value of u occur will give a segmentation result, a contour as the boundary of an object.

A contour $C \subset \Omega$ is implicitly represented by the zero level set of a Lipschitz function $\phi : \Omega \rightarrow \mathbb{R}$ in the level set method (Osher and Sethian, 1988); $C = \{(x, y) \in \Omega : \phi(x, y) = 0\}$. The optimal contour of the segmentation is attained by the evolution of the

embedding function $\phi(x, y, t)$ at time t and the process amounts to solving a partial differential equation (PDE) in the level set method; $\frac{\partial \phi}{\partial t} = 0$.

Chan and Vese model an image as $u(x, y) = c_1 H(\phi(x, y)) + c_2 \{1 - H(\phi(x, y))\}$, $(x, y) \in \bar{\Omega}$, where c_1 and c_2 are constants, and H is the Heaviside function. The constants c_1 and c_2 are in fact the average values of intensity where $\phi \geq 0$ and $\phi < 0$, respectively.

To find an optimal piecewise constant function to approximate the image, they evolve an embedding function ϕ minimising the energy functional $\mathcal{F}(c_1, c_2, \phi)$ for appropriate parameters $\mu \geq 0$, $\lambda_1 > 0$ and $\lambda_2 > 0$;

$$\begin{aligned} \mathcal{F} &= \mu \int_{\Omega} \delta(\phi(x, y)) |\nabla \phi(x, y)| dx dy & (2) \\ &+ \lambda_1 \int_{\Omega} |u_0(x, y) - c_1|^2 H(\phi(x, y)) dx dy \\ &+ \lambda_2 \int_{\Omega} |u_0(x, y) - c_2|^2 \{1 - H(\phi(x, y))\} dx dy, \end{aligned}$$

where δ is the 1D Dirac measure (as the weak derivative of H). The functional is a particular case of the Mumford-Shah minimal partition problem (Mumford and Shah, 1989). In order to solve the minimization problem using variational calculus, we used the approximation $H_{\epsilon} \in C^2(\bar{\Omega})$ of the Heaviside function H and its derivative δ_{ϵ} in the energy function \mathcal{F} as in (Chan and Vese, 2001): $H_{\epsilon}(z) = \frac{1}{2} (1 + \frac{2}{\pi} \arctan(\frac{z}{\epsilon}))$, $\delta_{\epsilon}(z) = \frac{\epsilon}{\pi(\epsilon^2 + z^2)}$. Note that $\lim_{\epsilon \rightarrow 0} H_{\epsilon} = H$. The Euler-Lagrange equation associated to the approximation to equation (2) is led to

$$\begin{aligned} \frac{\partial \phi}{\partial t} &= 0 \quad \text{in } (0, \infty) \times \Omega, & (3) \\ (IC) \quad \phi(0, x, y) &= \phi_0(x, y) \quad \text{in } \Omega, \\ (BC) \quad \frac{\delta_{\epsilon}(\phi)}{|\nabla \phi|} \frac{\partial \phi}{\partial \vec{n}} &= 0 \quad \text{on } \partial \Omega, \end{aligned}$$

where \vec{n} denotes the exterior normal to the boundary $\partial \Omega$, and $\partial \phi / \partial \vec{n}$ denotes the normal derivative of ϕ at the boundary. The partial derivative in the PDE (3) is

$$\frac{\partial \phi}{\partial t} = \delta_{\epsilon}(\phi) \left[\mu \operatorname{div} \left(\frac{\nabla \phi}{|\nabla \phi|} \right) - \lambda_1 (u - c_1)^2 + \lambda_2 (u - c_2)^2 \right].$$

The level set model with $\epsilon = 1$ is used to segment the mesorectum as well as candidates of lymph node.

2.3 Automatic 3D Lookup from 2D Data Set

If the proposed methods are fully automatic, they would be more practical. This subsection discusses implementation criteria of automatic lookup to make our methods fully automatic.

The proposed methods of lymph node analysis can be implemented with three stages: segmentation using a level set method, a lookup of candidates; analysis of the candidates with a Gaussian estimate.

The level set method described in the previous subsection is also used for delineation of lymph candidates on an image. The zero level set results in numerous blobs on the image, and from them we must select candidates of lymph nodes to analyse. The level set implementation and Gaussian fitting proposed in this section can be automatic. If we can make the selection of candidates from the zero level set automatic, the whole process will be fully automatic.

In section 2.1 we suggested intensity as a classification criterion of lymph nodes where Gaussian fitting is utilised. There are other classification criteria to be considered for lymph nodes and they will be included in our automatic lookup stage.

In the clinical studies of lymph nodes (Brown et al., 2003; Lee et al., 1984), large lymph nodes are a sign of malignancy; 60% of involved lymph nodes are 4mm diameter or larger in 2D images. We try to look up even smaller blobs than this cilncal criterion of size, which is based on human vision.

We look for candidates, 3D blobs, by reading 2D images. Therefore, we need to consider connectivity of 2D blobs between slices. For the connectivity, we consider geometric structure of anatomy appeared on 2D image slices and provide a criterion of distance. If a dark blob extends over a consecutive slice of thickness 3mm and it runs at an extreme slope through slices, it could be located as far as 8 pixel distance on the consecutive slice of a $0.39mm \times 0.39mm$ pixel size; 4 pixel distance for a $0.78mm \times 0.78mm$ pixel size. Since patients remain still during an MR scan and there is very little motion due to breathing, we do not need to consider motion effect in the images. Therefore, this geometric criterion is reasonable.

In the next section, the models summarised in this section are implemented on MR images.

3 EXPERIMENTS

The images used in our experiments are T_2 weighted MR colorectal images stored in DICOM format. They are scanned off-plane and oblique axial thin section as shown in Figure 1. Angulation of a scan plane perpendicular to the rectum is known in general to give better information than other standard image planes such as coronal and sagittal since the rectum is at an angle. All images tested in this paper were scanned either at John Radcliffe Hospital or Churchill Hospital, Oxford, UK. The parameters used in the 1.5T MR

scanner were TE = 120ms, TR = 6500ms, flip angle = 90° . Each slice of a sequence is taken at a uniform distance.

Due to strong edges of neighbouring organs in contrast to extremely thin edges of the mesorectal fascia, we crop the images as in Figure 1 to a smaller field of view than those shown in the left of Figure 2.

For our purposes, lymph node detection and characterisation, we need to segment three objects from images: the mesorectum, colorectum and a lymph node candidate scattered in the mesorectum. Among the various level set models that we have tested, such as edge stopping, geodesic, and bandwidth, the model of (Chan and Vese, 2001) showed better performance on our images than other models. Their 2D model has been found to be better than its 3D generalisation or multi-phase model for our images.

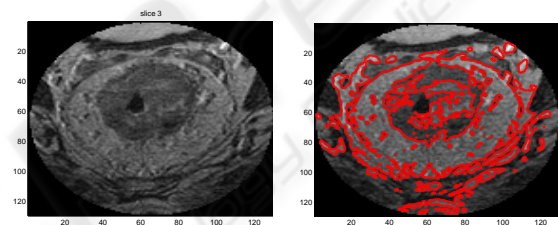


Figure 2: A small field of view MR slice(left); its segmentation results of a level set method (right).

Subsection 3.1 presents the detection and characterisation of a single candidate of lymph node. The methods are extended to the automatic detection of all possible candidates in subsection 3.2; a validation issue is discussed in subsection 3.3.

3.1 A Single Candidate of Lymph Node

The first example set is presented in the left column of Figure 3. The data set is a sequence of consecutive slices of 3mm thickness and the pixel size is $0.78mm \times 0.78mm$.

As described in section 2, we employed the model of Chan and Vese and the resulting zero level set of an optimal solution of the differential equation (3) was obtained as presented in Figure 2 (right).

Then we organise the zero level set and selected the contours delineating the three objects as presented in the right column of Figure 3 at each corresponding row. In the figures in the right column, the mesorectum is delineated as the region enclosed by two closed contours (red) for each of three images; the inner contour is the boundary of the colorectum and the outer contour the mesorectal fascia. A lymph node candidate is delineated by the green contour in the second

and third figure. In this case, as a result of our method, an individual lymph node candidate is examined.

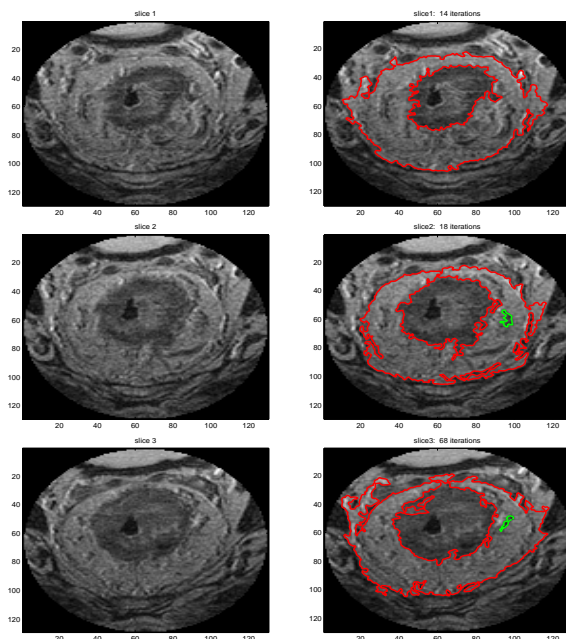


Figure 3: A set of consecutive MR slices with a small field of view (left column); their corresponding mesorectal contours selected from segmentation results by level set (right column). Mesorectal contours and colorectal contours are red, and a lymph node candidate green.

Our segmentation results enabled us to build a PDF and to use it to detect lymph nodes as outliers, as described in section 2. We collect the intensity values of the mesorectal fascia of the MR slices to learn its voxel PDF. The voxel intensity histogram is depicted in Figure 4 (blue stem and head). The optimal parameters of the Gaussian distribution are $\mu = 190.986$ and $\sigma = 40.924$. The optimal fit, with these parameters is depicted by a red curve in Figure 4. Two vertical lines for the values of $\mu - \sigma$ (solid line) and $\mu - 2\sigma$ (dotted line) on the horizontal axis are also plotted in the figure for the purpose of demonstration of our criterion.

Now we collect the intensity values of the lymph candidate whose planar sections are depicted by green contours in Figure 3. The histogram of the lymph candidate (pink heads) is overlaid on the histogram of the voxel intensity of the mesorectum, which appears around the $\mu - 2\sigma$, at the left tail of the red Gaussian curve in Figure 4. The mean intensity of the lymph candidate is computed. The value is 118.709 and is slightly larger than $\mu - 2\sigma$. These values are summarised in Table 1 for comparison.

We have also tested datasets at a higher resolution, i.e. images about four times bigger than the dataset

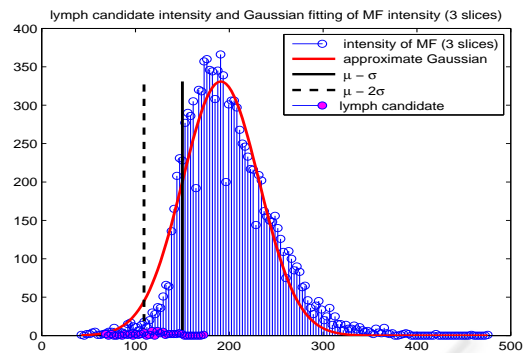


Figure 4: The histogram of the intensity of the mesorectum of the three slices, delineated in Figure 3 (blue stem) and its Gaussian estimate (red curve). The histogram of the intensity of a lymph node candidate is overlaid (pink heads), which is clustered around $\mu - 2\sigma$.

Table 1: Comparison of lymph node candidate to the parameters of Gaussian in Figure. 4

| mean (lymph candidate) | $\mu - 2\sigma$ | $\mu - 1.5\sigma$ | $\mu - \sigma$ |
|------------------------|-----------------|-------------------|----------------|
| 118.709 | 109.138 | 129.600 | 150.062 |

presented in Figure 3. The slice thickness of this example set is $3mm$ and pixel size is $0.39mm \times 0.39mm$. The four images are in Figure 5. The selected contours from the segmentation results using the level set method are presented in the figure.

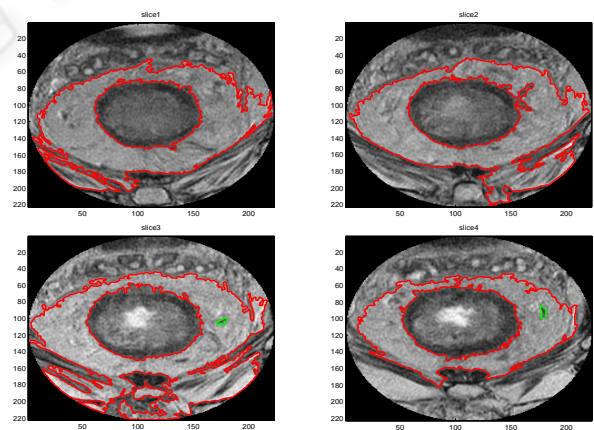


Figure 5: A set of consecutive MR slices with a small field of view and their mesorectal contours selected from segmentation results by level set. Mesorectal contours and colorectal contours are red, and a lymph node candidate green.

The intensity of the segmented mesorectum of the dataset is approximated by a Gaussian distribution in Figure 6; the estimated parameters are $\mu = 336.906$ and $\sigma = 45.488$. For this example, the mean intensity

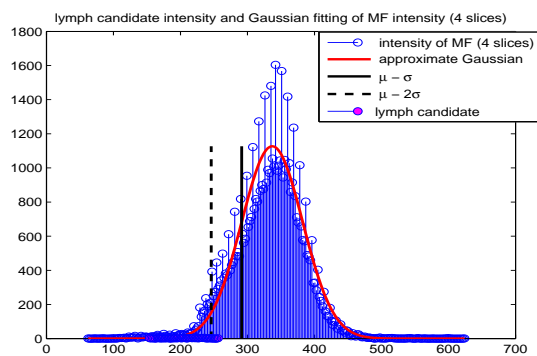


Figure 6: The histogram of the intensity of the mesorectum of the four slices, segmented in Figure 5 (blue stem) and its Gaussian estimate (red curve). The histogram of the intensity of a lymph candidate is overlaid (pink heads), which is clustered below $\mu - 2\sigma$ at the left tail of the Gaussian.

of the lymph node candidate seen in Figure 5 is computed as 206.245. The comparison of the intensity of the lymph node to the intensity of the mesorectal fascia is given in Table 2. In this dataset, the mean intensity of the lymph candidate is far smaller than $\mu - 2\sigma$.

Table 2: Intensity comparison of lymph node candidate to the parameters of Gaussian in Figure 6.

| mean (lymph candidate) | $\mu - 2\sigma$ | $\mu - \sigma$ |
|------------------------|-----------------|----------------|
| 206.245 | 245.929 | 291.417 |

If we define the criterion of lymph node to be smaller than $\mu - 1.5\sigma$, then the two individual candidates tested in this subsection are outliers of Gaussians and are classified as lymph nodes.

3.2 Multiple Candidates of Lymph Node

We extend the methods for a single candidate presented in subsection 3.1 to all possible candidates.

In the first example set in subsection 3.1, we organised the zero level set to select possible candidates from a few dozens to a hundred small blobs per image. The candidates which are located within the mesorectum and not very tiny are selected. Considering the criteria discussed in subsection 2.3, we set the thresholds of the size of possible candidates and of the distance for connectivity over slices. Our aim is to provide more scientific methods and try to capture small lymph nodes which can be missed by human vision. Hence, we select all blobs of 3mm diameter (i.e. 11 pixels of size $0.78mm \times 0.78mm$) or larger and they are candidates. The candidates are then analysed with

their Gaussian estimates individually, as done in section 3.1.

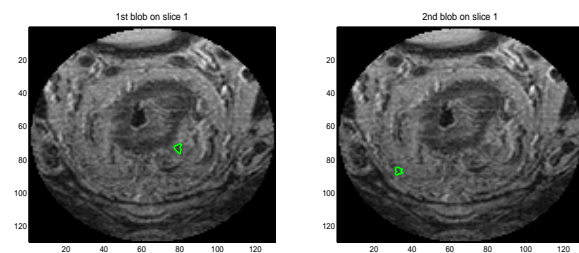


Figure 7: Single blobs found as candidates (green).

In this example of three slices, we selected 14 candidates from our lookup and some of them are presented in Figure 5 (appeared on consecutive slices in the right column) and Figure 7 (appeared on a single slice). The intensity of each candidate is grouped and its mean intensity is computed. The mean intensity values of these 14 candidates are plotted in the horizontal bar chart in Figure 8. In the figure, seven candidates are outliers of the Gaussian distribution in Figure 4 and estimated as lymph nodes as suggested in section 2. Some of the seven lymph nodes are depicted in Figure 9.

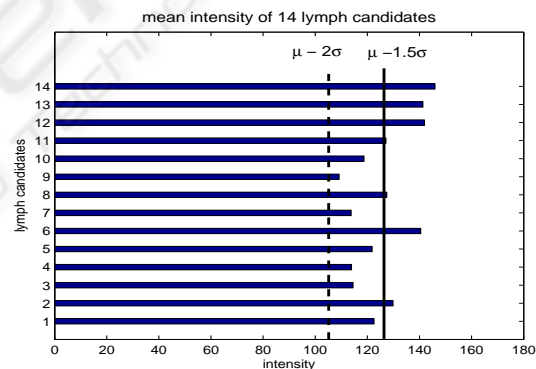


Figure 8: The mean intensity of detected candidates of the three slices in Figure 3 are collected and their mean intensity is plotted in the bar chart. Only seven candidates are below $\mu - 1.5\sigma$ of the Gaussian (solid vertical lines).

For the second example set in section 3.1, the same procedure is carried out. In this example of four slices, we selected five candidates; some of them are shown in Figure 10 as well as Figure 5. The mean intensity values of these five candidates are plotted in the horizontal bar chart in Figure 11; all the candidates are outliers of the Gaussian distribution in Figure 6 and estimated as lymph nodes.

We also tested a number of examples in which we performed manual segmentation. In all these experiments (of both automatic and manual segmentation),

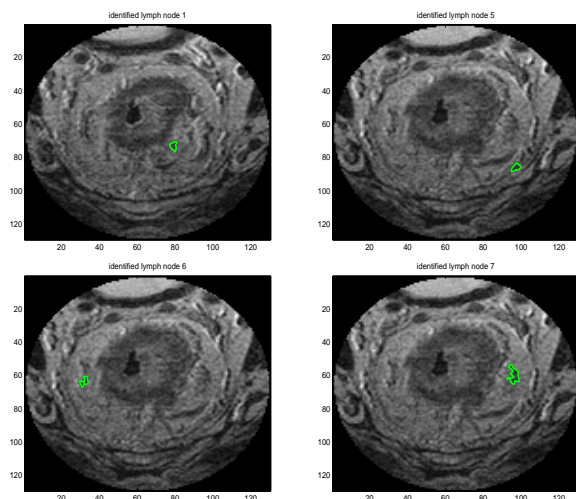


Figure 9: Candidates classified as lymph nodes (green).

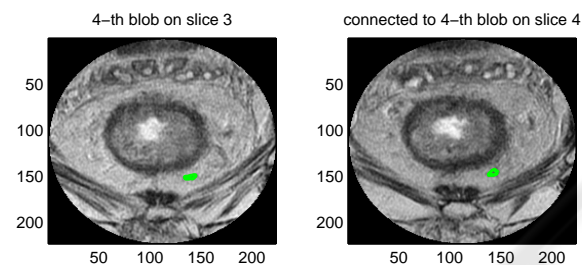


Figure 10: Blobs selected as a candidate (green); connected to consecutive slices.

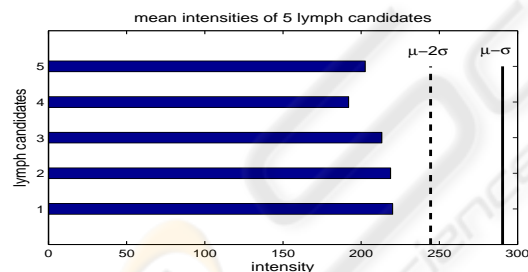


Figure 11: The mean intensity of detected candidates of the four slices in Figure 5 are collected and their mean intensity is plotted in the bar chart. they are all below $\mu - 2\sigma$ of the Gaussian (dotted vertical lines).

the mean values of intensity of lymph candidates are smaller than or slightly larger than $\mu - 2\sigma$. These experiments enable us to ascertain that a mean value of intensity is smaller than $\mu - 2\sigma$ but for a population set of a small size we need allow some margin of error in this criterion. For this reason, we suggest that candidate lymph nodes correspond to being outliers of the estimated Gaussian as

$$\text{mean}(\text{lymph intensity}) < \mu - 1.5\sigma$$

The estimation of the Gaussian of the mesorectum enabled us to provide an explicit criterion for the candidate to be classed as a lymph node. The whole process of the proposed methods is fully automatic.

3.3 Manual Segmentation of Lymph Candidates

We have compared our automatic method to manual segmentation for the example set in Figure 9. We detected five lymph nodes from our manually segmented candidates using the same criteria as in the automatic segmentation. Among the seven blobs classified as lymph nodes with automatic segmentation, four were also detected with manual segmentation. Note that this disagreement is not only due to the quality of automatic segmentation but due to the subjectivity of segmenting small objects.

An example enlarged is presented in Figure 12 which shows the difficulty of manual segmentation of a small object on a noisy image.

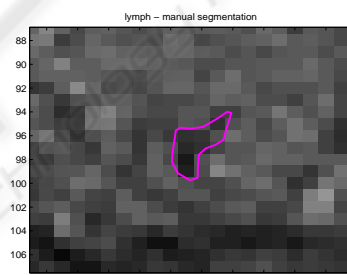


Figure 12: A manually segmented lymph candidate on a blurred image.

Another type of problems are demonstrated in Figure 13; the figure on the left hand side was automatically segmented, and the figure on the right hand side was manually segmented. The figure demonstrates the difference between machine vision (left) vs. human vision (right) to segment lymph candidates. The bump pointed by a broken arrow was segmented into the region of colorectum with automatic segmentation (left), but it was segmented manually as a dark blob near the boundary of the colorectum (right). The other two dark blobs pointed by solid arrows (left) were segmented automatically and were included in the set of our candidates; while they were merged into one object with manual segmentation (right), which can be classified as blood vessel rather than a lymph node candidate. These are the same problems as the current methods practiced by clinicians, heavily relying on human vision. Therefore, at this stage without further evidence, it is difficult to say if the three lymph nodes additionally de-

tected by automatic segmentation and our characterisation criterion are indeed false positives.

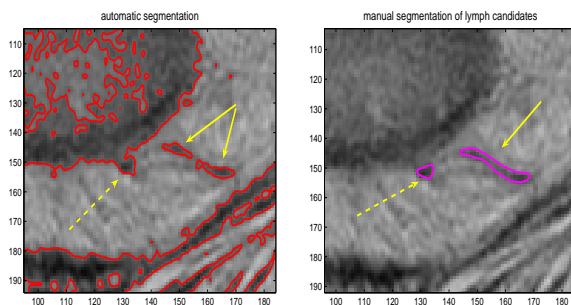


Figure 13: Differences between machine vision (left) vs. human vision (right) in segmenting lymph node candidates. Broken arrows: Part of the colorectum (left) or a blob (right)? Solid arrows: two blobs (left) or blood vessel (right)?

4 CONCLUDING REMARKS AND DISCUSSIONS

We have proposed methods to characterise and detect lymph nodes in MR colorectal images. Using a level set method, we were able to delineate the boundaries of the mesorectal fascia, colorectum, and a lymph node candidate from non-trivial images. With the delineated boundaries, we estimated the intensity PDF of the mesorectum, and approximated it by a Gaussian distribution. The intensity of the segmented lymph node candidate was then compared to the Gaussian distribution. We suggest that lymph nodes can be detected as outliers of the estimated Gaussian, with a mean intensity smaller than $\mu - 1.5\sigma$. This provides a more scientific means of lymph node characterisation. The implementation is fully automated.

The number, size, and location of lymph node candidates on each slice vary. In our data sets, the thickness of slice (usually from 3mm to 5mm) is quite large in comparison to the pixel size ($0.78\text{mm} \times 0.78\text{mm}$ or $0.39\text{mm} \times 0.39\text{mm}$). We cannot capture the true information between slices and this may keep from precise detection using information on images. For example, learning the 3D connectivity of lymph candidates between 2D slices is not straightforward unless they are sufficiently big. Since we implement a region merging algorithm individually for 2D slices and the slice thickness is often larger than the lymph node size, a high possibility of missing information exists. However, for small dark blobs that are prone to be missed by human vision are able to be detected by the proposed methods.

As discussed in subsection 3.3, validation is not

straightforward to carry out. Considering that pathologists routinely find more nodes in the dissected specimen than reported by radiologists, a true validation of a lymph node detection is very difficult.

Though better than the other segmentation methods examined, our level set implementation was not always successful; leaking occurred when edges were extremely thin and strong edges were nearby, as seen in some slices in section 3.1 figures. Our characterisation criterion of lymph nodes (Gaussian distribution thresholding) might not be sufficient. We think our work is an initial study for more scientific methods of cancer staging and hope it promotes the active study of lymph node detection using image analysis approaches.

Some clinicians use signal heterogeneity as a lymph characteristic. In our data sets, this was not the case and thus we did not consider it in this paper. However, for a large study population, this could be taken into account in combination with the proposed methods. Another plausible, yet highly involved method may be to analyse the signal change and heterogeneity of a lymph node where contrast agent is used. These could be the subjects of our ongoing work.

ACKNOWLEDGEMENTS

This work was supported by GE.

REFERENCES

- Bond, S. (2006). *Image analysis for patient management in colorectal cancer*. PhD thesis, Oxford university, Oxford, UK.
- Brown, G., Richards, C., Bourn, M., Newcombe, R., Radcliff, A., Dallimore, N., and Williams, G. (2003). Morphological predictors of lymph node status in rectal cancer with use of high-spatial-resolution mr imaging with histopathologic comparison. *Radiology*, 227:372–377.
- Caselles, V., Kimmel, R., and Sapiro, G. (1997). Geodesic active contours. *Int. J. Comp. Vis.*, 22:61–79.
- Chan, T. and Vese, L. (2001). Active contours without edges. *IEEE Trans. on Image Processing*, 10(2):266–277.
- Cremers, D. (2006). Dynamical statistical shape priors for level set based tracking. *IEEE Trans. PAMI*, 28(8):1262–1273.
- Felsberg, M. and Sommer, G. (2001). The monogenic signal. *IEEE Transactions on Signal Processing*, 49(12).
- Filippone, A., Ambrosini, R., Fuschi, M., Marinelli, T., Genovesi, D., and Bonomo, L. (2004). Preoperative t

- and n staging of colorectal cancer. *Radiology*, 231:83–90.
- Lee, J., Heiken, J., Ling, D., Glazer, H., Balfe, D., Levitt, R., Dixon, W., and Murphy, W. (1984). Magnetic resonance imaging of abdominal and pelvic lymphadenopathy. *Radiology*, 153:181–188.
- Lee, S. and Seo, J. (2006). Level set-based bimodal segmentation with stationary global minimum. *IEEE Trans. on Image Processing*, 15(9):2843–2852.
- Li, C., Xu, C., Gui, C., and Fox, M. (2005). Level set evolution without re-initialization: A new variational formulation. In *CVPR*, pages 430–436.
- Malladi, R., Sethian, J., and Vemuri, B. (1995). Shape modeling with front propagation: a level set approach. *IEEE Trans. PAMI*, 17(2):158–175.
- Marroquin, J. L., Santana, E., and Botelto, S. (2003). Hidden markov measure field models for image segmentation. *IEEE Trans. PAMI*, 25(11):1380–1387.
- McArdle, C., Kerr, D., and Boyle, P. (2000). *Colorectal Cancer*. Isis medical Media Ltd.
- Mumford, D. and Shah, J. (1989). Optimal approximation by piecewise smooth functions and associated variational problems. *Commun. Pure Appl. Math.*, 42:577–685.
- Osher, S. and Sethian, J. (1988). Front propagating with curvature-dependent speed: algorithms based on hamilton-jacobi formulation. *J. Comput. Phys.*, pages 12–49.
- Paragios, N. and Deriche, R. (2000). Geodesic active contours and level sets for the detection and tracking of moving objects. *IEEE Trans. PAMI*, 22(3):266–280.
- Perona, P. and Malik, J. (1990). Scale-space and edge detection using anisotropic diffusion. *IEEE Trans. PAMI*, 12(7):629–639.
- Sethian, J. (1999). *Level Set Methods and Fast Marching Methods: Evolving Interfaces in Computational Geometry, Fluid Mechanics, Computer Vision and Materials Science*. Cambridge University Press.
- Sung, J., Lau, J., Goh, K., and Leung, W. (2005). Increasing incidence of colorectal cancer in asia: implications for screening. *The Lancet Oncology*, 6(11):871–876.
- Yezzi, A. and Soatto, S. (2003). Stereoscopic segmentation. *Int. J. of Comp. Vis.*, 53(1):31–43.